PHILOSOPHICAL TRANSACTIONS OF THE ROYAL SOCIETY A MATHEMATICAL, PHYSICAL & ENGINEERING SCIENCES

The Breakdown of Superfluidity in Liquid ^{4}He: II. An Investigation of Excitation Emission from Negative Ions Travelling at Extreme Supercritical Velocities

T. Ellis, P. V. E. McClintock, R. M. Bowley and D. R. Allum

Phil. Trans. R. Soc. Lond. A 1980 **296**, 581-595
doi: 10.1098/rsta.1980.0195

THE BREAKDOWN OF SUPERFLUIDITY IN LIQUID ^{4}He II.† AN INVESTIGATION OF EXCITATION EMISSION FROM NEGATIVE IONS TRAVELLING AT EXTREME SUPERCRITICAL VELOCITIES

By T. ELLIS‡, P. V. E. McCLINTOCK‡, R. M. BOWLEY§ and D. R. ALLUM‖

‡ *Department of Physics, University of Lancaster, Lancaster LA1 4YB, U.K.*
§ *Department of Physics, The University, Nottingham NG7 2RD, U.K.*
‖ *Department of Physics, University of Exeter, Exeter EX4 4QL, U.K.*

(*Communicated by W. F. Vinen, F.R.S. – Received 9 August 1979*)

CONTENTS

We have measured the drift velocity, $\bar{v}$, of negative ions in He II at a temperature of 0.34 K and a pressure of 25 bar¶ for electric fields, E, in the range $5 \times 10^3 < E < 6 \times 10^6$ V m^{-1}. For $\bar{v} < 70$ m s^{-1}, the results are in good agreement with the predictions of the roton pair-emission theory of Bowley & Sheard. Even better agreement is obtained by extending the theory to take explicit account of departures from parabolicity of the real dispersion curve at large momenta, variations in the pole strength of high momentum excitations, and the slight increase in the average momentum of excitations emitted at large values of $\bar{v}$. For $\bar{v} > 70$ m s^{-1}, however, experiment and theory are in clear disagreement: by $\bar{v} = 80$ m s^{-1}, the measured drag on the ion has become about 100 % larger than the theoretical prediction. We tentatively attribute this discrepancy to the onset at $\bar{v} \approx 70$ m s^{-1} of a new and, so far, unidentified dissipation mechanism.

† Part I appeared in *Phil. Trans. R. Soc. Lond.* A **284**, 179–224 (1977).
¶ 1 bar = 10^5 Pa.

1. Introduction

In an earlier paper (Allum *et al.* 1977), hereinafter referred to as I, it was reported that negative ions can be drawn through superfluid ^{4}He at speeds, $\bar{v}$, significantly in excess of the Landau critical velocity, v_L, for roton creation under the influence of relatively modest electric fields, E. An unexpected outcome of these experiments was the discovery that the functional form of $\bar{v}(E)$ was apparently inconsistent with the drag on the ion being provided mainly by single-roton emission processes, as had been anticipated: for single-roton emission a characteristic of the form $(\bar{v}-v_L) \propto E^{\frac{2}{3}}$ would be expected, whereas the experimental data were rather accurately described by $(\bar{v}-v_L) \propto E^{\frac{1}{3}}$. A possible explanation of this discrepancy was suggested by Bowley & Sheard (1975, 1977), who pointed out that if, for some reason, single-roton emission did not occur, the ion would continue to accelerate until two-roton emission became energetically allowed. As discussed in I, they were able to show that this hypothesis leads to $\bar{v}(E)$ behaviour precisely of the form observed experimentally. Working on the premise that two-roton emission was the dominant process, they calculated the form of $\bar{v}(E)$ to be expected for a very wide range of electric fields.

Although the experimental results described in I can be regarded as strong evidence in favour of the two-roton emission hypothesis, no satisfactory explanation has yet been offered as to why pair emission should apparently be preferred in this way. It is highly desirable, therefore, that the Bowley–Sheard (B.S.) theory should be subjected to further experimental tests. Two substantial tests have been suggested, both involving the measurement of $\bar{v}(E)$ in electric fields not attainable by means of the apparatus of I. First, by investigating ion motion in extremely weak electric fields it may be possible to detect the occurrence of single-roton emission, if it exists: the theory predicts in detail the behaviour to be expected of $\bar{v}(E)$ in the transition region between two-roton and single-roton dominance, and it is even possible that a region of negative resistance may be discovered if the relative strengths of the two processes are sufficiently different from each other (Sheard & Bowley 1978). Such measurements are being planned, but will not be discussed further here. Secondly, in very strong electric fields, large departures are expected from the simple $(\bar{v}-v_L) \propto E^{\frac{1}{3}}$ behaviour observed for the fields of up to 3×10^5 V m^{-1} used in I. Preliminary high field measurements (Allum *et al.* 1976) suggested good agreement with the theoretical prediction, but were of inadequate precision to enable a satisfactory comparison to be made up to the highest fields used.

In this paper we present the results of experiments in which we have measured $\bar{v}(E)$ up to $E = 6 \times 10^6$ V m^{-1} with sufficient precision to search for possible departures from the characteristic predicted by the B.S. pair-emission theory. Such deviations would be expected if, for example, multi-roton processes, in which several rotons are emitted simultaneously from the moving ion, were allowed and could occur at a rate comparable with that of two-roton emission.

2. Experimental details

The basic techniques developed for injecting negative ions into pressurized superfluid helium and for measuring their drift velocities have already been described in I. In extending the measurements to very much stronger electric fields, it has however been necessary to introduce a number of modifications; these we discuss below. All the measurements were performed at 0.34 K, where, for the electric fields in question, $\bar{v}$ is temperature-independent.

(*a*) *The ion cell*

Four electrode structures and two experimental chambers were successively designed, constructed and mounted in the cryostat as the work developed towards higher electric fields, but only the final system, used for all the measurements to be presented below, will be described. It is illustrated diagrammatically in figure 1. It differs from that of I principally by virtue of its very short drift space, nominally 1 mm in length, so that a field of 5×10^6 V m^{-1} could be achieved by applying a potential difference of 5 kV. The diameter of the space traversed by the ions was much larger, being 20 mm rather than 10 mm. The ratio of diameter to length was such that no field-homogenizing electrodes were required.

For such a relatively short chamber, it was, of course, particularly important that the grids and collector should be accurately aligned and that the grids should be tightly and evenly stretched on their carriers. A special jig was designed to facilitate the mounting of the grids, enabling them to be stretched to their yield point and then held securely while being fixed in position by means of silver conducting paint. The grids themselves were of nickel, whereas the carriers were constructed from mild steel, which, by virtue of its smaller coefficient of thermal contraction, ensured that the grids remained taut to the lowest temperatures.

Although the intended working field of 5×10^6 V m^{-1} was about an order of magnitude below the breakdown electric field, as measured between smooth hemispherical electrodes (Gerhold 1972), considerable difficulty was experienced with electrical breakdown inside the cell, often occurring at about 2×10^6 V m^{-1}. This was apparently a consequence of local field enhancement at the grid wires; the effect was substantially reduced by resorting to grids of a lower geometrical transparency. Even with this precaution, breakdowns still occurred occasionally, apparently initiated at the slightly excrescent edges of the grids where they were attached to their carriers. The problem was finally eliminated by adding an annular disk of nylon, 0.5 mm thick, to the inside of the nylon spacer that defined the length of the drift space, in such a way as to cover the regions of attachment (not shown in figure 1). The grids themselves were of a nominal 2000 wires per inch, 2.5 μm thick and of 25 % geometrical transparency. The hole size (6.4 μm) was very much smaller than either the gate (nominal 0.2 mm), G_3–C (nominal 0.1 mm) or drift space lengths and thus ensured that the electric fields in these regions could be uniform, as well as preventing any serious 'leakage' of the relatively high drift space field into the gate.

The actual electrode spacings, with estimated experimental uncertainties, as measured at room temperature were: G_1–G_2 = (0.21 ± 0.02) mm; G_2–G_3 = (0.92 ± 0.05) mm; G_3–C = (0.11 ± 0.02) mm. With allowance for thermal contraction in cooling to 0.3 K from room temperature, the effective cold length of the drift space G_2–G_3 in zero electric field was estimated to be (0.88 ± 0.05) mm.

(*b*) *Data acquisition*

Because the flight time of the ions across the drift space (12–20 μs) was to be more than an order of magnitude shorter than in I, it was necessary to employ a faster signal processing system. The current induced in the collector was taken to earth via a 2 kΩ resistor, the 'high' side of which was connected to a Brookdeal 9454 amplifier, the output of which was then passed to a Biomation 8100 transient recorder. The digitized signal from the latter was transferred to a Nicolet Instruments LAB80 minicomputer for averaging and subsequent analysis. The sequence in which voltage pulses were applied to the tip and the gate was the same as was described in I. The repetition rate for the measurement cycle was usually set at 5 Hz.

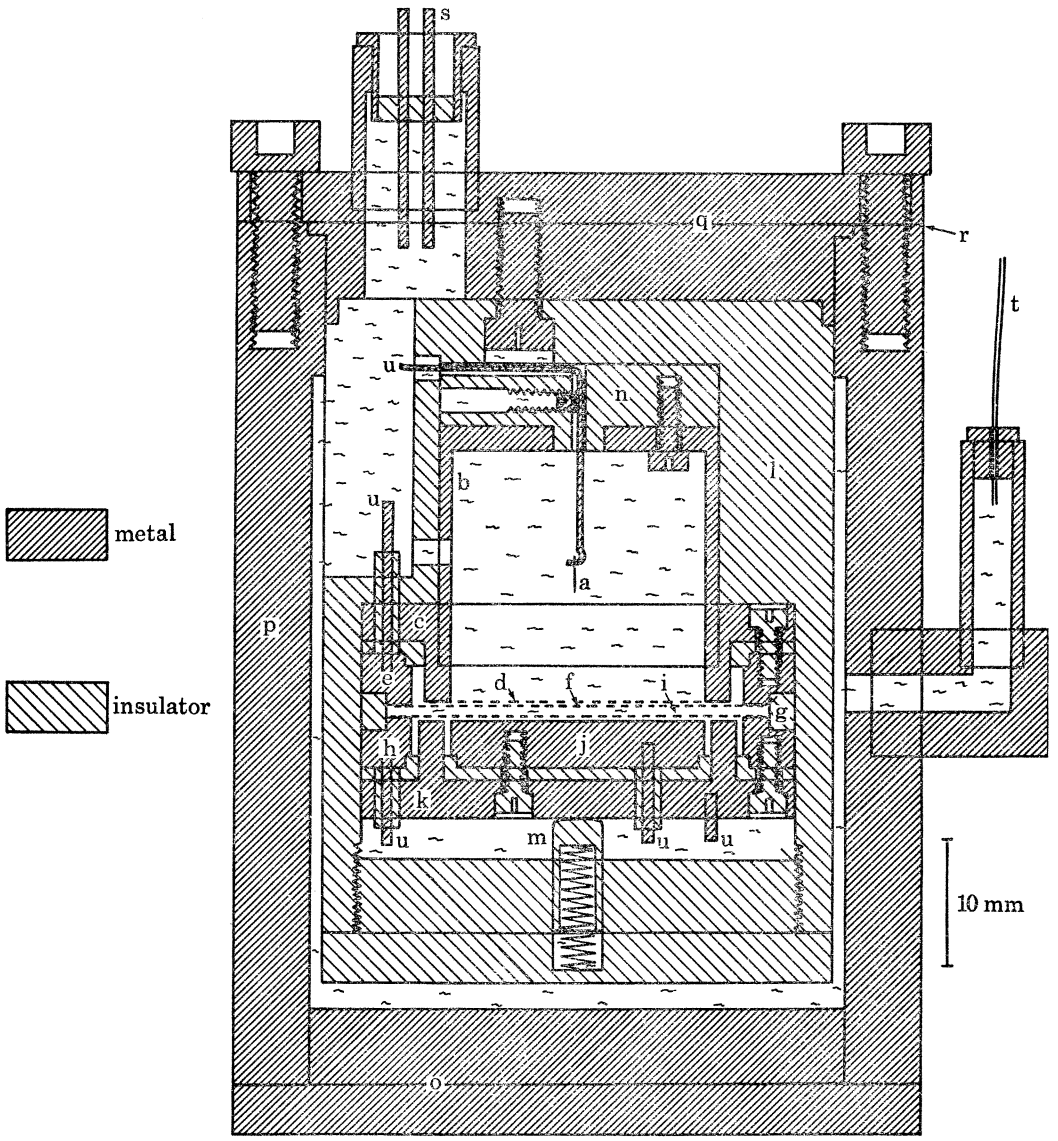

FIGURE 1. The experimental chamber, slightly modified so as to appear in a single vertical section. The principal components are all cylindrically symmetrical. a, Tungsten field emitter, spot-welded to nickel support wire; b, brass backplate; c, mild steel electrode to carry G_1, in electrical contact with backplate; d, nickel grid G_1; e, mild steel electrode to carry G_2; f, nickel grid G_2; g, nylon ring to define separation of grids G_2 and G_3; h, mild steel electrode to carry G_3; i, nickel grid G_3; j, mild steel collector; k, mild steel base and guard ring for collector assembly; l, nylon electrode holder; m, spring-loaded nylon plunger in lid of electrode holder; n, nylon holder for field emitter, with grub screw to secure nickel support wire; o, copper base of chamber; p, brass wall of chamber; q, brass lid of chamber; r, indium 'O' ring seal, placed inside the ring of M4 steel bolts; s, one of four two-pin metal–glass seals; t, 0.1 mm inner diameter stainless steel capillary through which the sample entered the chamber; u, solder tag for interconnecting wires.

A difficulty arose from the tendency of the amplifier to ring slightly in response to transients; although the ringing amplitude was very small, being considerably less than the random electrical noise of the input stage, it was enhanced by the averaging process. In particular, the ringing induced by the gate 'off' transient tended to obscure the first arrival of the ion pulse at the collector. This particular difficulty was largely avoided by using gating pulses that were considerably

longer than the flight time of the ions, so that the 'on' and 'off' events were completely separated from each other.

Typically, 2000 signals were summed by the minicomputer; these were followed by a further 2000 signals, but with use of the negative differential input of the transient recorder and with the drift field switched off so as to eliminate the current at the collector. Although this procedure inevitably slightly degraded the intrinsic signal/noise, it substantially reduced the amplitude of the ringing, which could still be troublesome at very high electric fields, where the flight times were short.

(*c*) *Data analysis*

The signals were analysed digitally, by means of the minicomputer. The (idealized) signal shape displayed on the monitor oscilloscope after averaging had been completed was as in figure 2, where the various characteristic timing points have been labelled so as to preserve consistency with the nomenclature of I. The analysis procedure started with the identification by channel number of the gate transients at t_1 and t_2. Least squares fits were then made to the linear parts of the signal on either side of t_3 and of t_5 to determine the equations of these lines. The

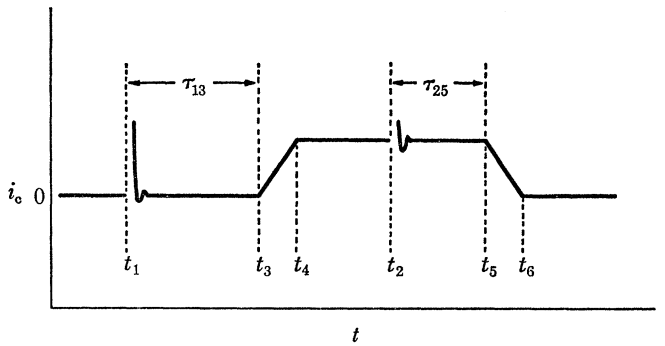

FIGURE 2. The (somewhat idealized) signal expected at the collector. The collector current i_c is plotted as a function of time t. Transients caused by the field emitter switching are not shown. The characteristic times are: t_1, a negative gate opening pulse is applied to G_1; t_2, the gate shuts again; t_3, the leading edge of the cloud of negative ions reaches G_3; t_4, the leading edge of the ion cloud reaches the collector; t_5, the trailing edge of the ion cloud reaches G_3; t_6, the trailing edge of the ion cloud reaches the collector. The intervals τ_{13} and τ_{25} correspond respectively to the times taken by an ion in travelling from G_1 to G_3 and from G_2 to G_3.

equations were solved to find numerical values of $\tau_{13} = t_3 - t_1$ and of $\tau_{25} = t_5 - t_2$, corresponding respectively to the times taken by the ions to travel from G_1 to G_3 and from G_2 to G_3. As the length, l, between G_2 and G_3 is known, the velocity, $\bar{v}$, of the ions in the drift space could then be calculated.

The transient tagging and the definition of those regions of the signal to which straight lines were to be fitted were accomplished by means of a pair of electronic cursors. Once these procedures had been completed, the rest of the operation was entirely automatic and values of $\bar{v}$ and τ_{13} were printed out on the teletype. The gradient and intercept for each fitted line, together with the corresponding standard deviations, were also printed. Finally, the digital signals were recorded on magnetic 'floppy' disk to permit subsequent reanalysis, should this prove to be desirable.

It was necessary to apply three corrections to values of $\bar{v}$ measured in this way. First, the positions of the gate transients were checked. In doing so, a few gate pulses, in place of the ion pulse, were passed via an attenuator into the transient recorder; the channel numbers

corresponding respectively to the gate opening and shutting were noted and then compared with those deduced from the immediately preceding averaged signal. The difference seldom amounted to more than one channel (0.05 μs), and was usually zero. Where necessary, small adjustments were made to $\bar{v}$ and τ_{13}. The need for this procedure was occasioned by the ringing cancellation technique described above (which, if completely successful, would have eliminated the gate transients altogether).

Secondly, explicit allowance was made for the finite rise time of the signal circuit. A separate experiment was performed in which a signal, similar in both shape and magnitude to that due to the ions, was passed into the signal system via the collector lead, and then, subsequently, via an attenuator, directly into the transient recorder. In each instance the standard signal analysis routine was followed, but with both cursors set on channel zero instead of on the usual transients. The differences in τ_{13} and τ_{25}, each measured in these two different ways (0.35 ± 0.02) μs, gave a direct measure of the effect of the finite rise time on the positions of t_3 and t_5 as determined by the fitting procedure used in practice. Appropriate small adjustments were then made to $\bar{v}$ and to τ_{13}.

Finally, a correction was made to allow for grid movement when the electric field in the drift space was large: G_2 and G_3 are drawn towards each other, each taking up an equilibrium profile in the form of a paraboloid. It is straightforward to demonstrate that, for small deflections, the distance moved by the centre of each grid is

$$\delta x = 0.13\epsilon_0 R^2 E^2/aTn,$$

where R is the radius of the grid, E the difference in electric field on either side of the grid, T its tension, a the cross-sectional area of a grid wire, and n the number of grid wires per unit length. Inserting the appropriate dimensions for our particular chamber and taking for T the room temperature yield stress of about 10^8 N m^{-2}, we find

$$\delta x \approx 10^{-18}E^2, \tag{1}$$

where E is in volts per metre and δx in metres. The change in the effective length of the drift space might therefore be *ca.* 5 % at the highest fields used, so that this correction is likely to be quite important. In practice, of course, T was not accurately known, and we have preferred to measure the change in l experimentally by investigating the variation with E of the ionic transit times across G_1–G_2 and across G_3–C, as described in § 3.

3. Experimental results

Some typical collector signals, both before and after the averaging process had been completed, are shown in figure 3. They bear quite a close resemblance to the idealized signal shape of figure 2, apart from some pulse droop arising from the limited low-frequency response of the signal circuit. The decrease in the ionic transit time τ_{25} with increased drift space electrical field, E_d, is clearly evident. Residual ringing of the amplifier became more severe at high electric fields (figure 3*h*), perhaps because the movements of G_2 and G_3 interfered with the efficacy of the ringing cancellation procedure described in § 2*b*.

The amplitude of the collector current varied by a factor of about two with changing E_d, as shown in figure 4. Qualitatively similar behaviour was observed in I, and was attributed principally to changes in the vortex nucleation rate ν, with E_d. Measured values of ν (Allum & McClintock 1978; Stamp *et al.* 1979) indicate, however, that vortex nucleation in the drift space cannot significantly affect i_c, the magnitude of the current pulse at the collector, for the very short

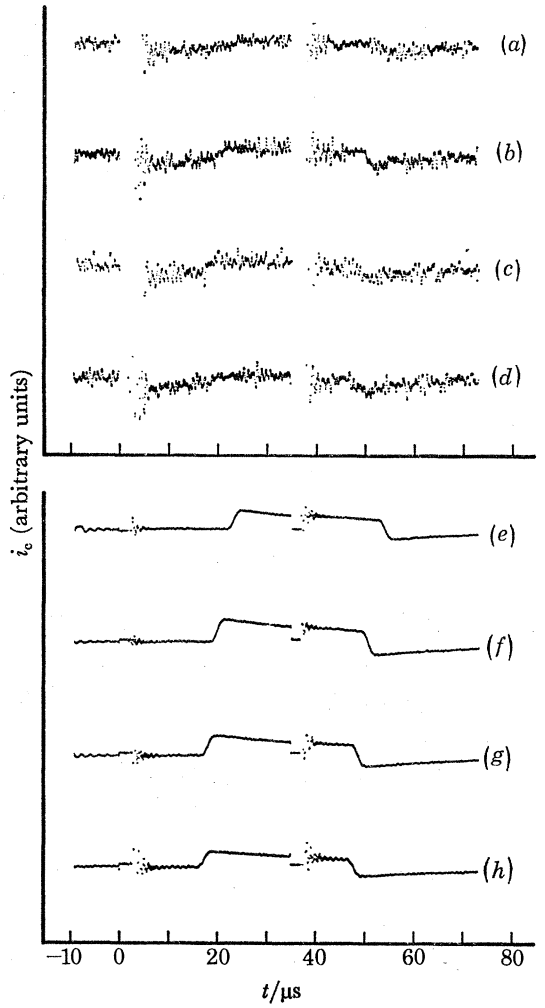

FIGURE 3. Typical signals received at the collector. The collector current i_c is plotted, in arbitrary units, as a function of time t from the opening of the gate. For absolute magnitudes of i_c at various values of the drift-space electric field E_d, see figure 4. Experimental parameters were: field emitter pulse potential, 2000 V; gate stopping potential difference, 5 V; gate opening pulse, 15 V, length, 35 μs, delayed 250 μs after field emitter pulse; sample pressure, 25 bar, and temperature, 0.34 K. Single sweeps for E_d values (in volts per metre) of: (*a*) 3.18×10^4; (*b*) 8.42×10^5; (*c*) 2.30×10^6; (*d*) 3.59×10^6. Final processed pulses, after signal averaging and the ringing reduction procedure, at E_d values of: (*e*) 3.18×10^4; (*f*) 8.42×10^5; (*g*) 2.30×10^6; (*h*) 3.59×10^6.

chamber used in the present experiments. Rather, we believe that the form of $i_c(E_d)$ shown in figure 4 is caused mainly by the effect of a varying mismatch of the electric fields on either side of G_2 and of G_3. When charge travels from a region of high E through a grid to a region of low E, the proportion collected by the grid is greater than might be expected on purely geometrical grounds because, in effect, a disproportionate number of electric field lines terminate on grid wires. In the reverse situation, where charge travels from a low E to a high E region, a disproportionate fraction of the charge is transmitted through the grid, whose effective transparency can even approach unity if the field mismatch is large enough. The latter effect is, of course, very much more pronounced for grids of low geometric transparency, as in the present instance.

The $i_c(E_d)$ characteristic of figure 4 can therefore be discussed as follows; the gate 'on' field

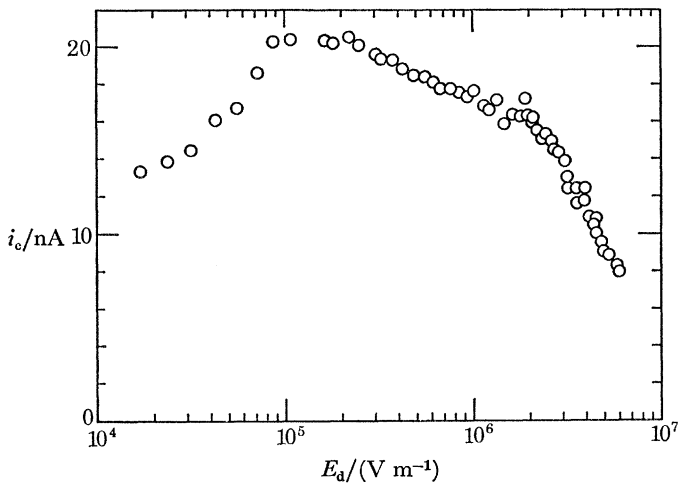

FIGURE 4. The absolute magnitude of the collector current i_c plotted as a function of the electric field E_d in the drift space, measured at time t_4 in each instance (see figure 2).

$E_g = 4.8 \times 10^4$ V m^{-1} and the G_3–C electric field $E_c = 1.25 \times 10^6$ V m^{-1}. Below 10^5 V m^{-1}, i_c is controlled mainly by the effective transparency, γ_g, of G_2, which decreases as E_d decreases; because $E_d \ll E_c$, the effective transparency, γ_c, of G_3 is close to unity. For $E_d > 10^6$ V m^{-1}, i_c is controlled mainly by γ_c, which will be about 0.25 at 1.6×10^6 V m^{-1} and which will decrease steadily with further increase of E_d; where $E_d \gg E_g$, $\gamma_g \approx 1$. The competing field dependences of γ_g and γ_c in $10^5 < E_d < 10^6$ V m^{-1} would lead to a relatively weak dependence of i_c on E_d in this region, as observed.

The gate transit time $\tau_G = \tau_{13} - \tau_{25}$ is plotted as a function of E_d in figure 5. There is a definite increase in τ_G above 10^6 V m^{-1}, which is attributable to an increase in the G_1–G_2 separation caused by the movement of G_2 (see § 2 (*c*)). The form of (1) suggests that the transit time will be given by

$$\tau_G = \tau_{Go} + AE_d^2, \tag{2}$$

where τ_{Go} is the gate transit time for very small E_d and A is a constant of order 3×10^{-14} if τ is in microseconds and E_d in volts per metre. In figure 6, the measured values of τ_G for $E_d > 10^6$ V m^{-1} are plotted against E_d^2; the form of the experimental results is clearly consistent with (2). An initial value of A having been obtained, the procedure was iterated and new values of E_d, corrected for the grid movement described by (2), were obtained. One iteration turned out to be sufficient and the values plotted in figure 5 correspond, in fact, to this first iteration. The full line represents a least squares fit of all the data to (2), yielding

$$\tau_G = (4.26 \pm 0.01) + (2.09 \pm 0.05) \times 10^{-14} E_d^2,$$

with τ_G in microseconds and E_d in volts per metre. The gradient is remarkably close to the value expected.

The ionic transit time from G_3 to C, $\tau_c = t_4 - t_3$, was also measured, and was also found to increase rapidly at the highest values of E_d. In this instance, however, the field on the other side of the grid was too large to ignore (E_c between G_3 and C was 1.25×10^6 V m^{-1}) and in fitting the data to (2) it was necessary to replace E_d with $(E_d - 1.25 \times 10^6)$. The result was

$$\tau_c = (1.83 \pm 0.02) \pm (2.0 \pm 0.3) \times 10^{-14} (E_d - 1.25 \times 10^6)^2,$$

when the $\pm$ sign between the terms is taken as positive when $E_d > E_c$ and negative when

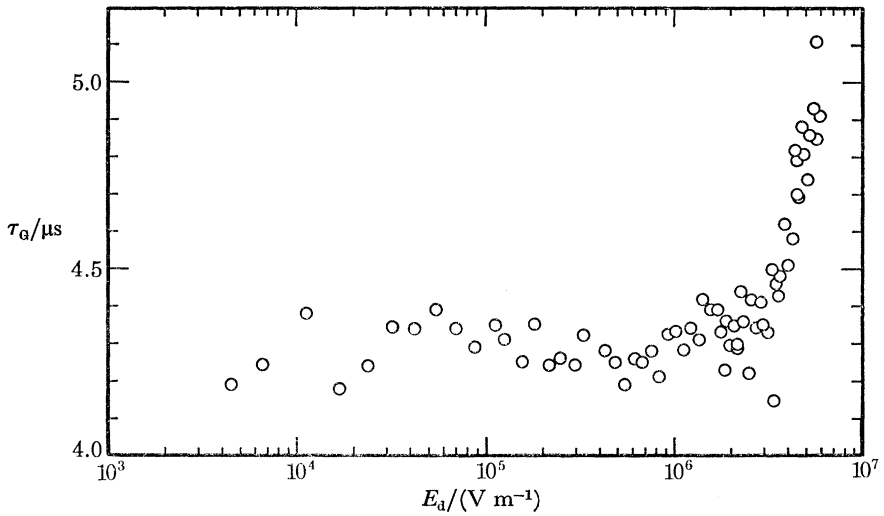

FIGURE 5. The gate transit time, $\tau_G = \tau_{13} - \tau_{25}$ (see figure 2), plotted as a function of the electric field E_G in the drift space. The rise in τ_G above $E_d = 10^6$ V m^{-1} is believed to be due to movement of G_2, which will be drawn towards G_3 for large values of E_d.

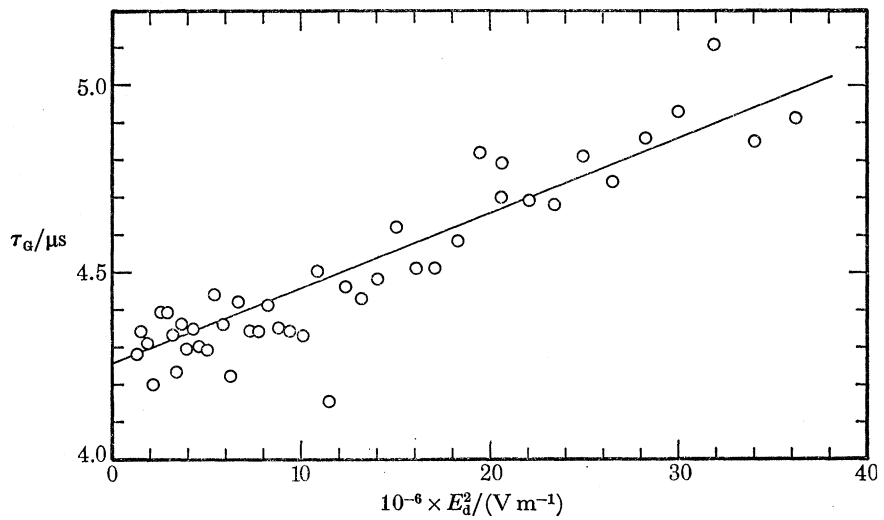

FIGURE 6. The gate transit time, τ_G, plotted against the square of the drift space electric field for comparison with equation (2). In the interests of clarity, only the data for $E_d > 10^6$ V m^{-1} have been plotted. The line represents a least-squares fit of equation (2) to the complete set of data, including those for $E_d < 10^6$ V m^{-1}

$E_d < E_c$. The statistical uncertainty in the intercept is greater because the amplitude of the movement was smaller for G_3 than for G_2. The gradient agrees, within experimental error, with that deduced for G_2.

The intercepts of 4.26 and 1.83 μs imply G_1–G_2 and G_3–C spacings of 0.22 and 0.12 mm respectively, in excellent agreement with the values deduced by measuring individual components at room temperature.

The measurements of $\bar{v}$, corrected for errors in transient tagging, for the finite rise time of the amplifier and for movement of the grids, are tabulated in the appendix and are plotted as a function of $E^{\frac{1}{3}}$, for more convenient comparison with the B.S. theory, in figure 7. The possible systematic errors in $\bar{v}$ and $\bar{E}$ arise mainly from uncertainties in the length, l, of the drift space and

PHILOSOPHICAL TRANSACTIONS OF THE ROYAL SOCIETY A MATHEMATICAL, PHYSICAL & ENGINEERING SCIENCES

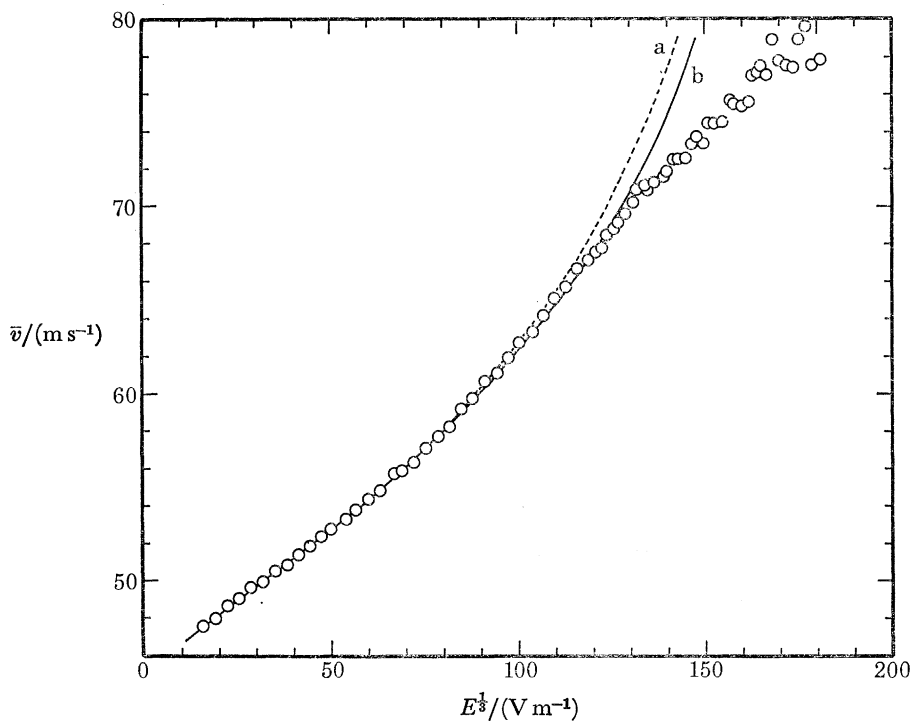

FIGURE 7. Measured values of the negative ionic drift velocity, $\bar{v}$, plotted as a function of (electric field, E)$^{\frac{1}{3}}$ for $P = 25$ bar, $T = 0.34$ K. The dashed curve a represents a fit of the Bowley–Sheard (B.S.) theory to the data points. The full curve b represents an extension of the B.S. theory to take account of non-parabolicity of the real dispersion curve, of the momentum dependence of the pole strength for excitations where k is far from k_0 and of the fact that the average momentum of the emitted excitations is slightly larger than hk_0 when $\bar{v}$ is large. It may be noted that the effect of the corrections to the B.S. theory is relatively small, that the extended theory is in excellent agreement with the data up to about 70 m s^{-1}, but that, for higher velocities, a large discrepancy develops.

are estimated at $\pm 6\,\%$. A measure of the random error in $\bar{v}$, arising principally from electrical noise on the received signals and the consequent uncertainties in the least squares fitting procedure used in analysis, is given by the scatter of the data points. The scatter is considerably larger for the highest velocities. This was partly because of the need to measure a shorter transit time, partly because the magnitude of the signals was smaller (figure 4) and partly because the absolute magnitude of the residual electrical noise increased with E_d (figure 3). The effects on $\bar{v}$ of altering the gate-open and -shut potential differences, the G_3–C potential difference and the emitter potential were carefully investigated, and were found to be zero within the scatter of the data.

4. DISCUSSION

Comparison of the experimental data with the B.S. theory (curve a of figure 7) confirms the excellent agreement found in earlier work below, $\bar{v} = 65$ m s^{-1}. At slightly higher velocities, the onset of small deviations can be seen, however, and at 70 m s^{-1} the experimental and theoretical characteristics separate quite abruptly. At our highest values of $\bar{v}$, the drag experienced by the ion is about 100 % larger than is predicted by the theory. The detailed shape of the experimental $\bar{v}(E^{\frac{1}{3}})$ curve is, of course, influenced by the correction that we applied to take account of grid movement, as described above. We believe, however, that the application of this correction is essential; this belief was apparently confirmed by the change in signal shape observed in high

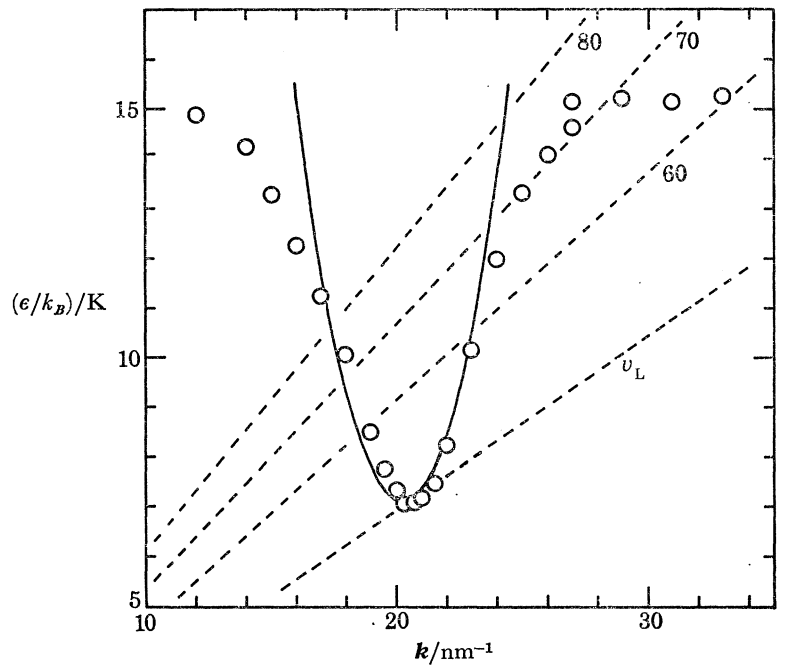

FIGURE 8. The high momentum part of the dispersion curve: the excitation energy ϵ is plotted as a function of its wave vector $\boldsymbol{k}$. The full curve is the parabola prescribed by equation (3), with accepted values of the roton parameters (Donnelly 1971) at 25 bar, and the points represent the neutron scattering data of Smith *et al.* (1977) at 24.3 bar. The pressure difference of 0.7 bar is not expected to be of any significance. The dashed lines are drawn from the origin, at gradients corresponding to the velocities given (in metres per second) by the adjacent figures in each instance, and they indicate the momentum range of the excitations, which is expected to be significant for the ionic drift velocities in question; on average, only the part of the dispersion curve that lies to the right of the line is accessible to the dissipation mechanism.

electric fields. It should be noted that, whereas our preliminary high field data (Allum *et al.* 1976) mostly fell above the theoretical curve, the more accurate data obtained in the present experiments, after application of all the relevant small corrections, clearly fall below it.

If we accept that the data of figure 7 are reliable, then we are forced to conclude that the B.S. theory fails for large values of $\bar{v}$. There are several reasons why we might have anticipated that this would be so. We discuss five of these below, together with possible ways in which the theory may be extended to render it more accurately applicable at high velocities.

(*a*) *Departures from parabolicity of the dispersion curve*

In the B.S. theory the density of states for the emitted excitations was calculated on the assumption that

$$\epsilon(k) = \Delta + \hbar^2(k-k_0)^2/2m_r, \tag{3}$$

where ϵ is the energy of an excitation of wave vector k and Δ, k_0 and m_r are roton parameters. For large velocities, such as are being considered here, it is energetically possible to create excitations far from the roton region, where (3) will not be applicable. In figure 8 we compare the curve corresponding to accepted values of the roton parameters (Donnelly 1971) that were used in the B.S. theory, with some recent neutron scattering measurements of the dispersion curve (Smith *et al.* 1977) at a pressure of 24.3 bar, very close to the 25.0 bar used in our experiments. Also included in the figure are (dashed) straight lines, drawn from origin, at gradients corresponding

to the indicated velocities. Since an ion can, in principle, create excitations at all points on the dispersion curve lying *below* the line corresponding to its average velocity, it is clearly quite essential that departures from parabolicity should be taken fully into account when $\bar{v} > 65$ m s^{-1}.

We also note from figure 8 that the value of k_0 is, in reality, slightly larger than that deduced from Donnelly's (1971) equations; in the calculations that follow, we have therefore taken $k_0 = 20.5$ nm^{-1}, which is consistent with the more up-to-date results of Smith *et al.* (1977).

The detailed shape of the dispersion curve is important for two reasons. First, it affects the average momentum of the emitted excitations; this point we discuss in more detail in §4(*c*). Secondly, it is clear from figure 8 that the density of states for excitations with $k \approx 30$ nm^{-1} will in reality be much larger than was tacitly assumed in the B.S. theory, which calculated the roton pair emission rate by means of

$$R(v) = \frac{\Omega^2 |V_0|^2}{(2\pi)^3 \hbar} \int k^2 \, \mathrm{d}k \int q^2 \, \mathrm{d}q \int_{-1}^{1} \mathrm{d}\mu \int_{-1}^{1} \mathrm{d}\mu' \, \delta(\bar{\epsilon}_k + \bar{\epsilon}_q - \hbar k v \mu - \hbar q \omega \mu'). \tag{4}$$

One might therefore expect that, if proper account were taken of the non-parabolic shape of the real dispersion curve where k is far from k_0, the excitation emission rate would become much larger, with a consequent increase in the drag experienced by the ion and a corresponding decrease in $\bar{v}$ below the value predicted by the B.S. theory. In fact, however, it is essential that the momentum dependence of the pole strength of the high k excitation also be considered. As discussed below, it turns out that an additional correction must be applied to the theory which, by de-emphasizing the influence of the high k part of the dispersion curve, greatly reduces the importance of the correction for non-parabolicity.

(*b*) *The pole strength for high momentum excitations*

The best model available for describing excitations with momenta of *ca.* 30 nm^{-1} is that given by Pitaevskii (1959); see also Zawadowski (1978) for a recent review. He assumes that the interaction of a quasiparticle of large momentum with two rotons gives the main contribution to the self energy of the excitation. The net effect is to alter the wave function and shift the energy of the excitation. A consequence is that the probability of creating one of these high momentum excitations is reduced by a factor $f(q)$, the pole strength. This quantity can be measured in neutron scattering experiments. It is found that, as the momentum increases and the flat part of the dispersion curve is approached, the pole strength vanishes. If the energy of an excitation is written

$$\epsilon = \epsilon_q^0 + \Sigma(q, \epsilon), \tag{5}$$

where $\Sigma(q, \epsilon)$ is the self energy, the pole strength is then

$$f(q) = \left(1 - \frac{\partial \Sigma(q, \epsilon)}{\partial \epsilon}\right)^{-1} \tag{6}$$

and the group velocity, which enters the formula for the density of states, is

$$\frac{\partial \epsilon}{\partial q} = \left(\frac{\partial \epsilon_q^0}{\partial q} + \frac{\partial \Sigma(q, \epsilon)}{\partial q}\right)\left(1 - \frac{\partial \Sigma(q, \epsilon)}{\partial \epsilon}\right)^{-1}. \tag{7}$$

To determine the corrected transition rate, we have weighted the integrals by the factor $f(q)f(k)$ and have also included the real (non-parabolic) excitation energies as measured by Smith *et al.* (1977) at 24.3 bar. We ignore the difference of 0.7 bar between their experiment and ours; it changes v_L by about 0.5 %, which is less than the scatter in the data. The integrations over q and

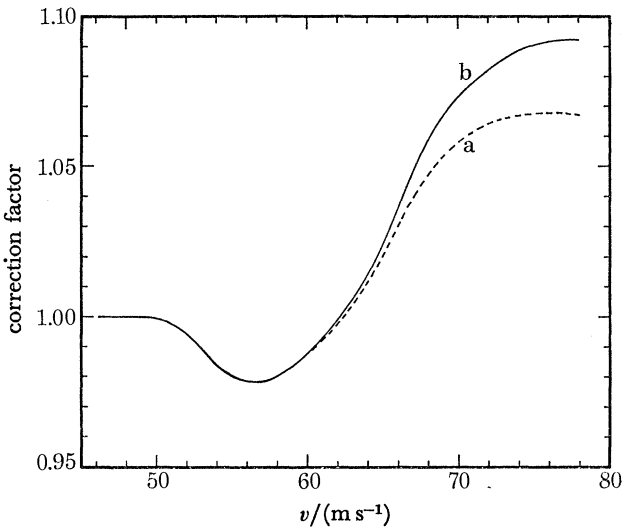

FIGURE 9. Corrections to the emission rate $R(v)$ used in the B.S. theory, as a function of ionic velocity v. Curve a represents the correction factor that must be applied to take account both of the non-parabolic nature of the real dispersion curve at high momenta (figure 8) and also of the momentum dependence of the pole strength of the excitations far from k_0. Curve b also includes an additional weighting factor, to make explicit allowance for the fact that the average momentum of the emitted excitations increases slightly above $\hbar k_0$ for large velocities of the ion.

k were computed by numerical methods, and those over μ and μ' were evaluated analytically. We have had to take values of the pole strength from experiments under the saturated vapour pressure (Cowley & Woods 1971) since measurements do not seem to have been reported for higher pressures, but the resultant correction to the transition rate turns out to be relatively insensitive to the exact values used.

In figure 9 we plot the ratio of the corrected emission rate to that calculated by Bowley & Sheard (curve a). It will be noted that the net change in $R(v)$, introduced by taking account simultaneously of the pole strength and of the real shape of the dispersion curve, is remarkably small. The reason for this is that the singular term $(1-\partial\Sigma(q,\epsilon)/\partial\epsilon)$ in the density of states (equation (7)) cancels with the identical term in equation (8) for the pole strength. The calculations could be in error, but the significant conclusion is just how small a change (*ca.* 10 %) in the predicted $R(v)$ follows from these two corrections. As pointed out above, a change tenfold larger than this would have been required to account for the measured values of $\bar{v}$ at high electric fields.

(*c*) *The average momentum of excitations emitted from the ion*

In evaluating the drag on the moving ion, the B.S. theory assumed that the average momentum of excitations emitted from the ion was $\hbar k_0$. Inspection of figure 8 suggests that, although this will be an excellent approximation for drift velocities only slightly in excess of v_L, it becomes progressively less accurate as $\bar{v}$ increases and is no longer tenable for our highest velocities, where the whole of the flat region of the dispersion curve near $30\,\mathrm{nm}^{-1}$ has become accessible to the dissipation mechanism. Here again, however, the pole strength factor de-emphasizes the influence of the high momentum part of the dispersion curve. A detailed calculation shows that the increase, above $\hbar k_0$, in the average momentum is 4 %, at most. Inclusion of this additional weighting factor gives curve b of figure 9.

This slight increase in the rate of momentum loss can be used to construct a corrected

theoretical curve. In principle, of course, we ought to repeat the B.S. calculation, including the new $R(v)$. In practice, however, the corrections are so small that it suffices to multiply the values of the drag given by Bowley & Sheard by the factor given by curve b of figure 9. The result is plotted as curve b of figure 7, which clearly fits the data closely over a very wide range of electric fields. The only remaining deviations are for $\bar{v} > 70$ m s^{-1}. These are relatively large and are clearly still in need of an explanation.

(*d*) *Momentum dependence of the matrix element*

The B.S. theory assumes that the matrix element $V_{q,k}$ for the emission of a pair of excitations is constant, irrespective of the magnitudes and directions of $\boldsymbol{q}$ and $\boldsymbol{k}$. The original justification for this assumption was that the emitted pair of rotons had roughly equal momenta, both lying almost parallel to the direction of motion of the ion. In the present instance, however, where we consider roton creation at very much higher ionic velocities, it is possible (indeed probable) that the matrix element varies significantly over the relevant range of momenta. To some extent, of course, we have already taken explicit account of this variation of $V_{q,k}$, through our inclusion of the pole strength factor $f(\boldsymbol{q})f(\boldsymbol{k})$.

We note, however, that any smooth variation of $V_{q,k}$ with $\boldsymbol{q}$ and $\boldsymbol{k}$ will be likely to lead to a smoothly varying $\bar{v}(E)$ curve. Indeed, the same would be true even if there was a discontinuous change in $V_{q,k}$, since the integrations over $\boldsymbol{q}$ and $\boldsymbol{k}$ tend to smooth out the variation of $R(v)$ with v. It seems unlikely, therefore, that the relatively sharp break at $\bar{v} \approx 70$ m s^{-1} between the data and the theoretical curve can be ascribed to a momentum dependence of the matrix element.

(*e*) *Other possible dissipative mechanisms*

It is, of course, possible that the ion dissipates energy via a new mechanism for velocities above about 70 m s^{-1}, this being related to the critical velocity for the process in question. For example, the simultaneous emission of more than two rotons might become important for $\bar{v} > 70$ m s^{-1}, and so also might the emission of phonons together with rotons. Dissipation involving the creation of vortex rings seems less probable because the attempt rate for the nucleation process is believed to be extremely small compared to the roton emission rate (Allum & McClintock 1978; Stamp *et al.* 1979) and because the very large electric fields in question will have annihilated completely the attractive potential (Donnelly & Roberts 1969) between the ion and the vortex, so that, even if the nucleation rate had in reality become large, it would be surprising if significant increments of momentum could be lost by the ion during such events.

5. Conclusion

We have found that, up to 65 m s^{-1}, measured values of $\bar{v}(E)$ are in good agreement with the predictions of the B.S. theory. The relatively small deviations found when 65 m s$^{-1} < \bar{v} < 70$ m s^{-1} are attributable to the combined effects of non-parabolicity of the real dispersion curve, momentum dependence of the pole strength, and departures from $\hbar k_0$ of the average momentum of the excitations emitted by the ion. When explicit allowance is made for these effects, the resultant theoretical curve is in excellent agreement up to $\bar{v} = 70$ m s^{-1}, thus lending further support to the roton pair-emission hypothesis of Bowley & Sheard.

For velocities above 70 m s^{-1}, however, the drag on the ion becomes much larger than predicted even by the corrected version of the theory, the discrepancy reaching 100 % for the highest

electric field used in the experiments, this discrepancy being very considerably in excess of the estimated experimental error. Particularly in view of the relatively sudden separation of the experimental and theoretical curves at 70 m s^{-1}, we may tentatively ascribe the discrepancy to the onset, at this velocity, of an additional dissipation process. This could involve multi-roton or phonon/roton emission or, alternatively, it might correspond to a completely novel mode of dissipation. The choice between these and other alternatives will clearly have to await further developments in the theory.

It is a pleasure to acknowledge the continuing assistance of Mr D. H. Bidle and Mr N. Bewley during the course of this research. The experimental work was supported by the Science Research Council (under GR/A/0388.3 and GR/A/4874.7) to whom one of us (D. R. A.) is also indebted for the support of a studentship.

Appendix: Tabular velocity data

A representative selection of the data recorded for a temperature of 0.34 K and a pressure of 25.0 bar is tabulated below.

E/(kV m^{-1})	$\bar{v}$/(m s^{-1})	E/(kV m^{-1})	$\bar{v}$/(m s^{-1})
4.54	47.50	2220	70.17
31.8	49.93	2660	71.6
107	52.39	3150	73.4
250	54.77	3590	74.5
488	57.71	3960	75.5
842	61.06	4490	77.2
1330	65.14	5400	78.9
1840	67.76		

References

Allum, D. R., Bowley, R. M. & McClintock, P. V. E. 1976 *Phys. Rev. Lett.* **36**, 1313–1316.
Allum, D. R., McClintock, P. V. E., Phillips, A. & Bowley, R. M. 1977 *Phil. Trans. R. Soc. Lond.* A **284**, 179–224.
Allum, D. R. & McClintock, P. V. E. 1978 *J. low Temp. Phys.* **31**, 321–338.
Bowley, R. M. & Sheard, F. W. 1975 *Proc. 14th Int. Conf. low Temp. Phys.* (ed. M. Krusius & M. Vuorio), vol. 1, pp. 165–168. Amsterdam, Oxford: North-Holland.
Bowley, R. M. & Sheard, F. W. 1977 *Phys. Rev.* B **16**, 244–254.
Cowley, R. A. & Woods, A. D. B. 1971 *Can. J. Phys.* **49**, 177–200.
Donnelly, R. J. 1971 *Phys. Lett.* A **39**, 221–2.
Donnelly, R. J. & Roberts, P. H. 1969 *Proc. R. Soc. Lond.* A **312**, 519–551.
Gerhold, J. 1972 *Cryogenics* **12**, 370–376.
Pitaevskii, L. P. 1959 *Soviet Phys. J.E.T.P.* **9**, 830–837.
Sheard, F. W. & Bowley, R. M. 1978 *Phys. Rev.* B **17**, 201–203.
Smith, A. J., Cowley, R. A., Woods, A. D. B. & Martel, P. 1977 *J. Phys.* C **10**, 543–553.
Stamp, P. C. E., McClintock, P. V. E. & Fairbairn, W. M. 1979 *J. Phys.* C **12**, L589–593.
Zawadowski, A. 1978 In *Proc. Int. Conf. Quantum Liquids* (*Erice*) (ed. J. Ruvalds & T. Regge). Amsterdam: North-Holland.